

Space charge formation in chromium compensated GaAs radiation detectors

E. Belas^{1*}, R. Grill¹, J. Pipek¹, P. Praus¹, J. Bok¹, A. Musienko¹, P. Moravec¹, O. Tolbanov², A. Tyazhev², A. Zarubin²

¹Charles University, Faculty of Mathematics and Physics, Institute of Physics, Ke Karlovu 5, Prague 2, CZ-12116 Czech Republic

²R&D Center “Advanced Electronic Technologies”, Tomsk State University, 36 Lenin av., Tomsk, 634050 Russia

*Corresponding author E-mail: eduard.belas@mff.cuni.cz

Abstract

Space charge formation in chromium-compensated GaAs sensors is investigated by the laser-induced transient current technique applying DC and pulsed bias. Formation of non-standard space charge manifested by an appearance of both negatively and positively charged regions in DC biased sensors was revealed during 5 ms after switching bias. Using Monte-Carlo simulations of pulsed current transients we determined enhanced electron lifetime $\tau = 150$ ns and electron drift mobility $\mu = 3650$ cm²/Vs. We developed and successfully applied theoretical model based on fast hole trapping in the system with spatially variable hole conductivity.

Keywords: GaAs, radiation detectors, TCT

1. Introduction

Semiinsulating (SI) GaAs compensated by in-diffused chromium (GaAs:Cr) appears nowadays a promising X-ray detector material overcoming known drawbacks of Liquid Encapsulated Czochralski (LEC) SI-GaAs significantly debased by EL2 defect [1-3]. GaAs:Cr exhibits extended electron lifetime and long-term stability at bias, conserving simultaneously profitable properties of GaAs-based room-temperature radiation detectors, especially the relatively high average atomic number ($Z=32$), moderate energy band-gap ($E_g=1.42$ eV) and high electron mobility ($\mu_e=6500$ cm²/Vs) [4-5]. One of the key problems for application of SI GaAs in high-performed radiation detectors is still space charge formation resulting in the internal electric field distortion.

In this paper we investigate GaAs:Cr sensors by the laser-induced transient current technique (L-TCT) [6] at pulsed and DC biasing [7], which enables us to evaluate the electron lifetime, the electron drift mobility, the charge collection efficiency, internal electric field evolution, and the space

charge formation. Current waveforms and their evolution are analyzed by Monte Carlo (MC) simulations considering the specific profile of the electric field, spreading of drifting charge by diffusion and surface recombination. Carriers trapping and detrapping are described by appropriate trapping time τ_T and detrapping time τ_D [8]. We suggested new model based on spatially variable hole conductivity consistent with all observed features and sample's characteristics and its conformity with experimental data is demonstrated. We demonstrate that using L-TCT the internal electric field distortion could be easily determined which gives direct feedback to growers for the optimization of the growth technology.

2. Experimental details

Planar detectors with dimensions 5 mm×5 mm×0.5 mm and one Hall bar sample with dimensions 3 mm×15 mm×0.5 mm were used for detailed

characterization of the material by measuring L-TCT and galvanomagnetic properties, respectively. Samples were cut from the SI GaAs:Cr single crystal wafer, which was prepared in the Tomsk State University in Russia by the Cr in-diffusion to both surfaces of the wafer [1,4]. Samples were mechanically polished using $1\ \mu\text{m}$ Al_2O_3 in aqueous suspension and Au/GaAs/Au contacts were prepared by the evaporation. Bulk resistivity $\rho_0=1.5\times 10^9\ \Omega\text{cm}$ was deduced from the Hall Effect measurement. The negative sign of the Hall coefficient together with rather low room temperature Hall mobility $1700\ \text{cm}^2/\text{Vs}$ indicates the mixed type of conductivity [9] and an important role of holes in the dark current. Such findings are in agreement with previously published data [1].

The semitransparent detector cathode was illuminated by the pulsed laser diode with above band-gap light at the wavelength $660\ \text{nm}$, which is absorbed in a thin layer $\sim 250\ \text{nm}$ under the cathode. Photo-generated electrons drift toward the anode and induce transient current whilst holes are immediately collected at the cathode and their effect may be neglected. The signal is amplified and recorded by a digital sampling oscilloscope at the frequency bandwidth $3\ \text{GHz}$. Neutral density filter is used for the laser intensity attenuation to suppress the photoelectron trapping and space charge formation by higher flux illumination. Biased pulse is correlated with the laser pulse position and pulsing conditions are defined by three parameters; laser pulse delay (LPD), bias pulse width (BPW) and depolarization time (DT), see Fig.1. The laser pulse with FWHM $\approx 0.5\ \text{ns}$ is delayed from the rising edge of the bias pulse for defined LPD.

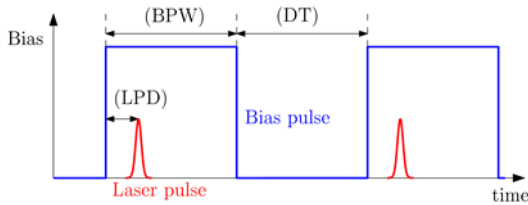


Fig.1. Scheme of the time correlation between the pulsed biasing and laser excitation.

Variable LPD allows us to visualize the progress of the internal electric field warping and evaluate the space charge formation by integrating the Gauss law.

3. Results and Discussions

Figs. 2a,b, show bias dependence of electron CWFs measured in planar GaAs:Cr detector using pulse and DC biased L-TCT, where pulsed bias parameters LPD= $80\ \mu\text{s}$, BPW= $10\ \text{ms}$ and DT= $10\ \text{ms}$ were chosen. High-frequency oscillations apparent at the initial stage of CWFs are caused by a response of the electronic circuit to the fast rising edge

of the current waveform and they are not analyzed in this paper. In both biases transit time of electrons drifting toward the anode was determined for the first time in this material. In the case of short LPD using pulsed bias, the space charge is not developed and we can consider detector nearly neutral with homogeneous electric field in the whole sample. Consequently, the CWF shape is affected only by the photoelectron trapping and recombination [7]. Representative Monte Carlo fits plotted by dashed lines in Figs. 2a,b were obtained with a model of two electron traps; one shallow trap characterized by trapping and detrapping time $\tau_{\text{TS}}=250\ \text{ns}$ and $\tau_{\text{DS}}=40\ \text{ns}$, respectively, and one deep trap with trapping time $\tau_{\text{TD}}=150\ \text{ns}$ and negligible detrapping. Electron drift mobility derived from the MC fit of each CWF resulted in $\mu_e=3650\ \text{cm}^2/\text{Vs}$. We observed also weak hole signal using anode illumination, but its structure was too fuzzy, that we could not determine transit time and other transport characteristics.

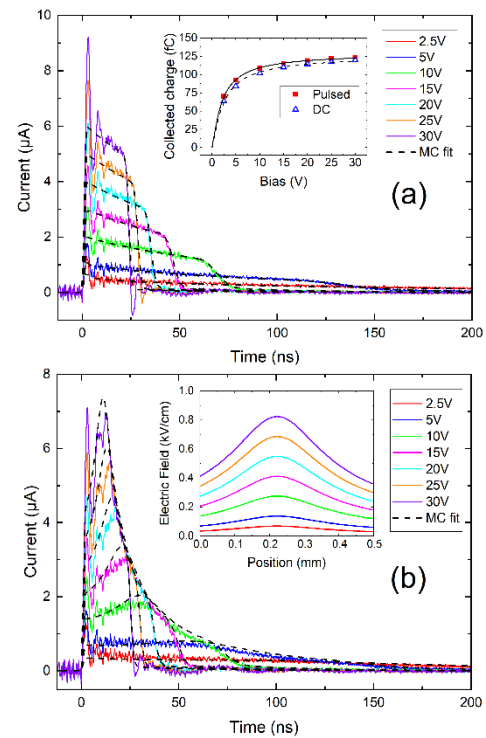


Fig.2. Bias dependence of electron current waveforms using a) pulse and b) DC biased L-TCT. Dashed lines represent the MC fit. The inset in the Fig.2a shows the bias dependence of collected charge evaluated by integration of CWFs applying pulsed and DC bias. Solid and dashed lines represent the Hecht equation fits. The inset in Fig.2b represents bias dependence of the internal electric field profile at DC bias.

In the case of DC L-TCT, we observed the non-standard shape of CWFs, which we did not observe in other materials nor noticed in the literature. We can clearly see in Fig. 2b that regardless of the magnitude of the biasing, CWFs

increase initially and after reaching maximum approximately at half of the electron transit time through the detector they decrease until electrons reach the anode. Such observation may be solely interpreted as an electron transport through the sample permeated by an ascending electric field, i.e. formation of the negative space charge region localized in the layer adjacent at the thickness about $L/2$ to the cathode, and by a descending electric field induced by positive space charge in the part near the anode.

Bias dependence of collected charge evaluated by the integration of the pulse and DC biased CWFs presented in Fig.2, is shown together with the Hecht equation fits in the inset in Fig.2a. We evaluated the electron mobility-lifetime products $\mu_e\tau_e^{Pulse} = 5.5 \times 10^{-4} \text{ cm}^2/\text{V}$ and $\mu_e\tau_e^{DC} = 5.2 \times 10^{-4} \text{ cm}^2/\text{V}$ from pulse or DC biased CWFs, respectively. Nearly linear scaling of the initial current transient with bias in the pulsed bias testifies on negligible electron surface recombination at the cathode. Let us note that in case of very low surface recombination, $\mu_e\tau_e^{Pulse}$ represents the right value of $\mu_e\tau_e$, which is untouched by electric field warping caused by the space charge formation resulting in the weak drop of $\mu_e\tau_e^{DC}$. For a comparison, applying pulse height spectrum analysis using alpha particles we obtained $\mu_e\tau_e^{alpha} = 1.4 \times 10^{-5} \text{ cm}^2/\text{V}$. Large difference between $\mu_e\tau_e^{Pulse}$ and $\mu_e\tau_e^{alpha}$ is caused by a strong plasma effect inducing strong photo-electron losses and the charge collection depression especially at low biases. Incorrect $\mu_e\tau_e^{alpha}$ value was also measured in [10] with the same interpretation. Bias dependence of the internal electric field profile representing the theoretical fit of DC CWFs is shown in the inset in Fig.2b.

The temporal evolution of CWFs measured at selected biases 10 V and 20 V by L-TCT with different LPD, see Fig. 1, is plotted in Fig. 3.

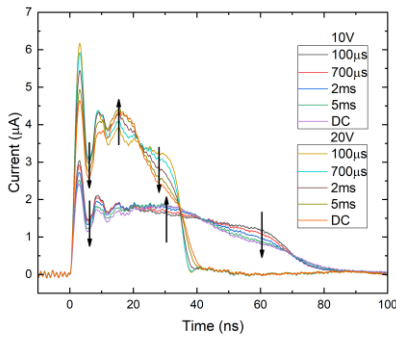


Fig.3. Electron L-TCT CWF dependence on the laser pulse delay for 10 V and 20 V pulsed biasing. Arrows show the direction of the waveform evolution.

We found that the CWF shapes continuously evolve after the biasing reaching the final form at LPD ≈ 5 ms. We clearly see that CWFs evolve continuously in their whole

shape, which proves that both positive and negative space charge regions are formed simultaneously.

The explanation of the simultaneous formation of both positive and negative space charge regions is a challenging task. Based on our previous investigations of the space charge formation in biased detectors [11] we conclude that obvious models explaining the space charge formation by appropriate contact properties cannot be applied in this material. New model should especially comply with the following results and known properties of SI GaAs:Cr material.

1. We measured significantly lower Hall mobility using Hall effect measurement in contrast to the electron drift mobility evaluated with the L-TCT, which testifies on the mixed type of the conductivity of GaAs:Cr and an important effect of holes at the transport. Comparable electron and hole conductivity $\sigma_e \approx \sigma_h$ may be assumed.
2. Weak L-TCT signal of holes was detected reflecting their very short lifetime and a significant hole trapping. Characteristic lifetime of holes $\tau_h < 3$ ns was estimated. Recently, $\tau_h = 1.4$ ns was reported [5] supporting such expectation.
3. SI GaAs:Cr wafer is prepared by Cr in-diffusion from the Cr layer applied to the both surfaces of the wafer. Due to this method, the residual variation of defect structure along the sample thickness can be assumed. Since Cr acts as an acceptor in GaAs:Cr, reduced/enhanced electron/hole density should appear near the surface in contrast to the middle of the detector. In other words, the Fermi energy E_F may be shifted towards the valence band in the subsurface regions relative to the middle of the detector. Variations at the resistivity similar to those considered here were presented in [1].

Based on the above-mentioned properties we developed a model considering the weak deviation of hole conductivity along the detector thickness, which consistently explain all observed features. Let us note that involving holes in the concept is important due to their short lifetime and consequently fast interaction with principal trap levels by the trapping and detrapping. Fast electrons with extended lifetime could not inspire observed formation of abruptly changing positive and negative space charge.

Since the mechanism of the Cr diffusion and defect compensation is not known in detail in GaAs:Cr yet, we expressed the course of hole conductivity profiled along the sample thickness by a nearly symmetrical trial function as follows

$$\sigma(x) = \sigma_0 + \sigma_1 \frac{(x-x_m)^2}{\sqrt{(x-x_m)^2 + \gamma^2}}, \quad (1)$$

where σ_0 , σ_1 , γ , and x_m are model parameters. Anticipating diffusion of Cr occurring from both sides of the wafer, $x_m \approx L/2$ is foreseen. Similar course may be deduced from the profile of resistivity [1].

Equation (1) is combined with obvious Ohm's law

$$j = \sigma E, \quad (2)$$

Gauss's law

$$\frac{\partial E}{\partial x} = \frac{\rho}{\epsilon} \quad (3)$$

and continuity equation

$$\frac{\partial \rho}{\partial t} = -\frac{\partial j}{\partial x} \quad (4)$$

where j , E , ρ , and ϵ are electric current density, electric field, charge density and permittivity, respectively. Eqs. (1)-(3) were substituted into eq. (4), which was numerically time integrated for given $\sigma(x)$. $E(x)$ was calculated by the integration of eq. (3) after each integration step with the boundary condition preserving the bias

$$U = -\int_0^L E(x) dx. \quad (5)$$

The cathode is set to $x=0$. Sample thickness $L=0.5$ mm. Basic properties of GaAs used at the calculations were taken from [12]. We used hole mobility $\mu_n=171$ cm²/Vs [3] and acquired $E(x)$ was applied in the MC simulation of experimental CWFs. Unique set of parameters was retrieved from the fitting of electron CWFs measured from both side of the sensor at variable bias in the interval 2.5 V-30 V and different laser time delay LTD 80 μ s – 5 ms as follows: $\sigma_0=2.2 \times 10^{-10}$ Ω^{-1} cm⁻¹, $\sigma_1=1.3 \times 10^{-8}$ Ω^{-1} cm⁻², $\gamma=0.1$ mm and $x_m=0.225$ mm. Fig.4 represents MC fit of L-TCT CWF dependence on the laser pulse delay for 20 V pulsed bias. Internal electric field profile in the detector is presented in the inset, where arrows show the direction of the electric field evolution.

Considering obtained results, the conductivity profile reaches its minimum at $x_m=0.225$ mm where $\sigma(x_m)=\sigma_0=2.2 \times 10^{-10}$ Ω^{-1} cm⁻¹ and maximum at the surface $\sigma(0)=4.4 \times 10^{-10}$ Ω^{-1} cm⁻¹; $\sigma(L)=5.2 \times 10^{-10}$ Ω^{-1} cm⁻¹. Respective position of Fermi energy $E_F(x_m)=E_V+0.689$ eV, $E_F(0)=E_V+0.672$ eV, and $E_F(L)=E_V+0.668$ eV. The space charge grows from its zero level at $t=0$ up to $\pm 4.5 \times 10^{10}$ cm⁻³ and $\pm 1.3 \times 10^{11}$ cm⁻³ at 10 V and 20 V, respectively, in DC bias. The hole and electron densities range from 8×10^6 cm⁻³ to 1.8×10^7 cm⁻³ and from 6×10^4 cm⁻³ to 1.4×10^5 cm⁻³, respectively, which is consistent with negative sign of the Hall coefficient with reduced measured Hall mobility

effected by mixed transport. The principle of the positive charging stems from weak injection of holes from the anode related with the larger hole conductivity and density in that region. Oppositely, the negative charge appears in the region adjacent to the cathode where the holes are depleted due to relatively lower conductivity in the middle of the sample, which inhibits the hole drift. It is worth to call attention to the fact that only two the most important parameters σ_0 and σ_1 allowed us to describe both the velocity of the space charge formation and the final magnitude of the space charge.

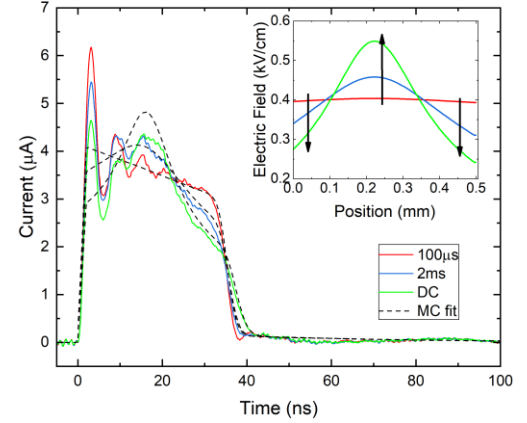


Fig.4. Electron L-TCT CWF dependence on the laser pulse delay for 20 V pulsed bias. Dashed lines represent the MC fit. The internal electric field profile in the detector is presented in the inset where arrows show the direction of the electric field evolution.

Simultaneously the fitted average conductivity of the sample $\langle \sigma \rangle = 3.2 \times 10^{-10}$ Ω^{-1} cm⁻¹ is close to the experimentally determined data and in agreement with mixed conductivity data.

4. Conclusion

We measured electron current transients in GaAs:Cr sensor using L-TCT in pulsed and DC bias and determined the time evolution of the space charge formation. We observed at the time scale of 5 ms gradual formation of both the negative space charge close to the cathode and simultaneously of the positive space charge near the anode, which limits charge collection efficiency of the sensor. Electron lifetime $\tau = 150$ ns and electron drift mobility $\mu = 3650$ cm²/Vs were evaluated from the Monte Carlo simulations. All experimental results have been explained within the model of variable hole conductivity caused by chromium diffusion. For elimination of the internal electric field distortion, pulsed bias application is recommended. We also showed that using L-TCT the internal electric field

profile could be easily determined which gives direct feedback to growers for the optimization of growth technology. We demonstrated that L-TCT allows researchers the non-destructive testing of transport properties in GaAs:Cr as well as in other radiation detector materials with much better precision than it may be reached by other commonly used techniques.

Acknowledgements

This work was supported by the Grant Agency of the Czech Republic under contract No. 18-12449S and by the Grant of the Charles University under contract No. SVV-2018-267306.

References

- [1] A.V. Tyazhev, D.L. Budnitsky, O.B. Koretskaya, V.A. Novikov, L.S. Okaevich, A.I. Potapov, O.P. Tolbanov, A.P. Vorobiev, *Nucl. Instr. and Meth. A* 509, 34 (2003).
- [2] I. Chsherbakov, I. Kolesnikova, A. Lozinskaya, T. Mihaylov, V. Novikov, A. Shemeryankina, O. Tolbanov, A. Tyazhev and A. Zarubin, *J. Instr.* 12, C02016 (2017)
- [3] J. Becker, M.W. Tate, K.S. Shanks, H.T. Philipp, J.T. Weiss, P. Purohit, D. Chamberlain and S.M. Gruner, *J. Instr.* 13, P01007 (2018)
- [4] G.I. Ayzenshtat, D.L. Budnitsky, O.B. Koretskaya, V.A. Novikov, L.S. Okaevich, A.I. Potapov, O.P. Tolbanov, A.V. Tyazhev, A.P. Vorobiev, *Nucl. Instr. and Meth. A* 487, 96 (2002).
- [5] D. Greiffenberg, M. Andrä, R. Barten, A. Bergamaschi, P. Busca, M. Brückner, S. Chiriotti Alvarez, I. Chsherbakov, R. Dinapoli, P. Fajardo, E. Fröjdh, C. Lopez-Cuenca, A. Lozinskaya, M. Meyer, D. Mezza, A. Mozzanica, S. Redford, M. Ruat, C. Ruder, B. Schmitt, X. Shi, D. Thattil, G. Tinti, O. Tolbanov, A. Tyazhev, S. Vetter, A. Zarubin and J. Zhang, *J. Instr.* 14, P05020 (2019)
- [6] P. Praus, E. Belas, J. Bok, R. Grill and J. Pekárek, *IEEE Trans. Nucl. Sci.* 63, 246 (2016).
- [7] A. Musiienko, R. Grill, J. Pekárek, E. Belas, P. Praus, J. Pipek, V. Dědič and H. Elhadidy, *Appl. Phys. Lett.* 111, 082103 (2017).
- [8] K. Suzuki, T. Sawada, and K. Imai, *IEEE Trans. Nucl. Sci.* 58, 1958 (2011).
- [9] D.C. Look, *J. Appl. Phys.* 48, 5141 (1977).
- [10] A. Tyazhev, V. Novikov, O. Tolbanov, A. Zarubin, M. Fiederle, E. Hamann, *Proc. SPIE* 9213, 92130G (2014).
- [11] R. Grill, E. Belas, J. Franc, M. Bugár, Š. Uxa, P. Moravec, and P. Höschl, *IEEE Trans. Nucl. Sci.* 58, 3172 (2011).
- [12] S. Adachi, *Properties of Group –IV, II-V and II-VI Semiconductors*, P.Capper, S. Kasap, A. Willoughby (Eds.), J. Willey & Sons Ltd (2005).